Structural and Kinetic Analysis of Miscoding Opposite the DNA Adduct 1,N^6-Ethenodeoxyadenosine by Human Translesion DNA Polymerase η*[S]

Amritraj Patra[1], **Yan Su**[1], **Qianqian Zhang**[1,2], **Kevin M. Johnson**, **F. Peter Guengerich**[3], and **Martin Egli**[4]

From the Department of Biochemistry, Vanderbilt University School of Medicine, Nashville, Tennessee 37232-0146

1,N^6-Ethenodeoxyadenosine (1,N^6-ϵdA) is the major etheno lesion formed in the reaction of DNA with epoxides substituted with good leaving groups (*e.g.* vinyl chloride epoxide). This lesion is also formed endogenously in DNA from lipid oxidation. Recombinant human DNA polymerase η (hpol η) can replicate oligonucleotide templates containing 1,N^6-ϵdA. In steady-state kinetic analysis, hpol η preferred to incorporate dATP and dGTP, compared with dTTP. Mass spectral analysis of incorporation products also showed preferred purine (A, G) incorporation and extensive −1 frameshifts, suggesting pairing of the inserted purine and slippage before further replication. Five x-ray crystal structures of hpol η ternary complexes were determined, three at the insertion and two at the extension stage. Two insertion complexes revealed incoming non-hydrolyzable dATP or dGTP analogs not pairing with but instead in a staggered configuration relative to 1,N^6-ϵdA in the *anti* conformation, thus opposite the 5′-T in the template, explaining the proclivity for frameshift misincorporation. In another insertion complex, dTTP was positioned opposite 1,N^6-ϵdA, and the adduct base was in the *syn* conformation, with formation of two hydrogen bonds. At the extension stage, with either an incorporated dA or dT opposite 1,N^6-ϵdA and 2′-deoxythymidine-5′-[(α,β)-imido]triphosphate opposite the 5′-A, the 3′-terminal nucleoside of the primer was disordered, consistent with the tendency not to incorporate dTTP opposite 1,N^6-ϵdA. Collectively, the results show a preference for purine pairing opposite 1,N^6-ϵdA and for −1 frameshifts.

Chemical or physical damage to DNA can lead to replication blockage and miscoding, which in turn can cause death or mutation of cells (1). Such changes can be associated with aging (2), cancer, and other diseases (3–6). Chemical damage to DNA can be the result of either exogenous (*e.g.* vinyl chloride (7)) or endogenous origin (*e.g.* oxygen radicals (8)). Some specific types of DNA damage can result from either exogenous or endogenous sources, as exemplified by the etheno (ϵ) adducts (9).

The etheno adducts are so named because they have an extra two carbons attached to DNA bases in an exocyclic arrangement (10). The history goes back to the chemistry of some unusual natural nucleosides found in tRNA, *e.g.* wybutosine and wyosine (11, 12), and also synthetic work by Leonard and co-workers, who utilized fluorescent etheno analogs to monitor biochemical phenomena (12–15). Barbin *et al.* (16) and Laib *et al.* (17) provided evidence that etheno adducts might be involved in the carcinogenicity of vinyl chloride, a known liver carcinogen in humans. Subsequent work showed the presence of etheno DNA adducts in rats that had never been exposed to vinyl chloride (or related vinyl monomers) (18) and that the adducts are the result of lipid peroxidation (19, 20). The reaction of the primary vinyl chloride oxidation product 2-chloroxirane with DNA yields 1,N^6-ethenodeoxyadenosine (1,N^6-ϵdA)[5] as the major etheno adduct (21), although the repair of this adduct is faster than that of some others, such that the N^2,3-ethenodeoxyguanosine levels become higher (22).

1,N^6-ϵdA has been incorporated into extrachromosomal vectors (23) and studied in cells. The adduct was reported not to be very mutagenic in *Escherichia coli* (23, 24), but this result may be due to extensive repair by the dioxygenase AlkB, which was later discovered to convert this lesion to deoxyadenosine (25). 1,N^6-ϵdA has been reported to be mutagenic in simian COS7 (24) and human HeLa, HCT116, and HEK293 cells (26, 27) and miscoding in human HeLa and XPV cell extracts (28). The bases A, C, and G have all been reported to be misinserted in these systems (24, 26–28) as well as T (*i.e.* no miscoding). Structural studies (NMR and x-ray) have been reported on oligonucleotides (in the absence of polymerases), with non-planar pairing between 1,N^6-ϵdA and dT and *anti* configurations of

both bases (29). 1,N^6-εdA:G pairing involved a *syn* configuration of 1,N^6-εdA and *anti* configuration of G (30). An x-ray crystallography study of 1,N^6-εdA:G pairing was interpreted to involve three H-bonds, with distortion of the oligonucleotide backbone to accommodate the pair (31).

Studies of misincorporation at 1,N^6-εdA have yielded varying results with individual DNA polymerases (pols). Singer *et al.* (32) reported that *E. coli* pol I and avian myelovirus reverse transcriptase inserted G, to some extent, but that dTTP incorporation was not blocked. When 1,N^6-εA was incorporated into an oligoribonucleotide, it was a complete block to avian myelovirus and Moloney murine leukemia virus reverse transcriptases (33). Human pol η (hpol η) was reported to bypass this lesion (34).

Levine *et al.* (34) reported that hpol η was 100-fold more active than hpol κ in replication past 1,N^6-εdA. We analyzed incorporation events using steady-state kinetics and LC-MS analysis of primers extended opposite 1,N^6-εdA by hpol η, in different sequence contexts. The results show hpol η bypass past 1,N^6-εdA in a highly error-prone manner, with a proclivity for incorporation of purines and generation of frameshifts. We also describe five x-ray crystal structures of hpol η ternary complexes, three containing 1,N^6-εdA paired with dTTP, dAMPNPP, or dGMPNPP (non-hydrolyzable dATP/dGTP analogs) at the insertion stage and two further structures of complexes at the extension stage, with either dA or dT opposite 1,N^6-εdA followed by a nascent pair between template A and an incoming dTMPNPP.

Results

Steady-state Kinetics of dNTP Incorporation Opposite A and 1,N⁶-εdA—To determine the efficiency and fidelity of translesion synthesis 1,N^6-εdA adducts by hpol η, steady-state kinetic analysis was performed. With an unmodified template (substrate B, Table 1), hpol η incorporated a single dNTP opposite A in the order of preference T ≫ A > G > C (Table 2), as expected. However, incorporation of dTTP opposite 1,N^6-εdA was very unfavorable, with a drastically decreased catalytic efficiency (1000-fold) compared with that of dTTP insertion opposite A (Table 2). In this study, dATP and dGTP were inserted more efficiently (3.7- and 2.5-fold, respectively, Table 2) than dTTP opposite 1,N^6-εdA. These results indicated that hpol η catalyzes translesion synthesis opposite 1,N^6-εdA in a very error-prone manner. Another sequence context containing 1,N^6-εdA (substrate C, Table 1), which had been used in a previous study by Levine *et al.* (34), was also included in our steady-state kinetic studies. Consistently, a high error rate for incorporation opposite 1,N^6-εdA by hpol η was observed, with preference for dGTP and dATP incorporation compared with dTTP (33- and 4.2-fold higher, respectively) (Table 3 and supplemental Fig. S1).

Pre-steady-state Kinetics—dNTP incorporation opposite 1,N^6-εdA was also examined in the sequence context of substrate A using a rapid quench method. However, no burst phase was observed with any of the four dNTPs, indicating that a step preceding nucleotidyl transfer is rate-limiting in all four cases (supplemental Fig. S2).

TABLE 1
Oligonucleotides used in this study
εdA is 1,N^6-εdA.

Oligonucleotides used in kinetic studies[a]

	Oligonucleotides
Substrate A	5´-(FAM)TCG TAA GCG TCA T -3´ 3´-AGC ATT CGC AGT A(εdA)C ACT-5´
Substrate B	5´-(FAM)TCG TAA GCG TCA T -3´ 3´-AGC ATT CGC AGT AAT ACT-5´
Substrate C	5´-(FAM)GTT CTA GCG TGT AGG TAT -3´ 3´-CAA GAT CGC ACA TCC ATA (εdA)CT CC-5´

Oligonucleotides used in LC-MS studies

	Oligonucleotides
Substrate A-U	5´-(FAM)TCG TAA GCG TCU T -3´ 3´-AGC ATT CGC AGT A(εdA)C ACT-5´
Substrate C-U	5´-(FAM)GTT CTA GCG TGT AGG UAT -3´ 3´-CAA GAT CGC ACA TCC ATA (εdA)CT CC-5´
Substrate D-U	5´-(FAM)TCG TAA GCG UCA T -3´ 3´-AGC ATT CGC AGT A(εdA)TACT -5´

Oligonucleotides used in the crystallization of hPol η:DNA complexes

Structure name	Oligonucleotides	Incoming nucleotide
εdA:dTTP	3´- TCG CAG TA(εdA) TAC -5´ 5´- AGC GTC AT -3´	dTTP
εdA:dAMPNPP	3´- TCG CAG TA(εdA) TAC -5´ 5´- AGC GTC AT -3´	dAMPNPP
εdA:dAMPNPP	3´- TCG CAG TA(εdA) TAC -5´ 5´- AGC GTC AT -3´	dGMPNPP
εdA:dT Extension	3´- TCG CAG T(εdA)G TAC -5´ 5´- AGC GTC AT -3´	dCMPNPP
εdA:dA Extension	3´- TCG CAG T(εdA)G TAC -5´ 5´- AGC GTC AA -3´	dCMPNPP

TABLE 2
Steady-state kinetics of incorporation of individual dNTPs opposite 1,N^6-εdA and A (Substrates A and B)

Substrate A	5´-(FAM)TCG TAA GCG TCA T -3´ 3´-AGC ATT CGC AGT A(εdA)C ACT-5´
Substrate B	5´-(FAM)TCG TAA GCG TCA T -3´ 3´-AGC ATT CGC AGT AAT ACT-5´

DNA Substrate	dNTP	K_m, μM	k_{cat}, min⁻¹	k_{cat}/K_m (μM⁻¹ min⁻¹)	f^a
Substrate A	dATP	29 ± 3	1.18 ± 0.02	0.041	3.7
	dGTP	36 ± 2	0.99 ± 0.01	0.027	2.5
	dCTP	433 ± 24	1.35 ± 0.03	0.0031	0.28
	dTTP	243 ± 36	2.61 ± 0.14	0.011	1
Substrate B	dATP	30 ± 2	7.9 ± 0.1	0.26	0.024
	dGTP	54 ± 5	7.8 ± 0.1	0.14	0.013
	dCTP	339 ± 21	7.6 ± 0.2	0.022	0.002
	dTTP	8.0 ± 0.5	89 ± 2	11	1

[a] Misinsertion frequency: $f = (k_{cat}/K_m)_{dNTP}/(k_{cat}/K_m)_{dTTP}$. The S.E. (±) is from the fit in Prism software.

LC-MS/MS Analysis of Primer Extension Products—In the steady-state kinetic analysis, hpol η showed a high misinsertion frequency opposite 1,N^6-εdA during single nucleotide extension (Tables 2 and 3). To gain insight into the ability of hpol η to

TABLE 3
Steady-state kinetics of incorporation of individual dNTPs opposite 1,N⁶-ϵdA within an alternate sequence context (Substrate C) (34)
The S.E. (±) is from the fit in Prism software. See Supplemental Data Fig. S1 for plots.

| Substrate C | 5′-(FAM)GTT CTA GCG TGT AGG TAT | | | −3′ |
| | 3′-CAA GAT CGC ACA TCC ATA (ϵdA)CT CC-5′ | | | |

DNA Substrate	dNTP	$K_m, \mu M$	k_{cat}, min^{-1}	$k_{cat}/K_m (\mu M^{-1} min^{-1})$	f
Substrate C	dATP	17 ± 2	3.3 ± 0.1	0.19 ± 0.02	4.2
	dGTP	1.4 ± 0.3	2.1 ± 0.1	1.5 ± 0.3	33
	dCTP	169 ± 20	2.8 ± 0.1	0.017 ± 0.002	0.38
	dTTP	124 ± 19	5.6 ± 0.2	0.045 ± 0.007	1

extend beyond the lesion, an LC-MS/MS method previously developed in this laboratory (34–36) and applied extensively (37–43) was used for sequence analysis of the extension products. dU-containing primers were extended by hpol η in the presence of all four dNTPs, followed by treatment with UDG and piperidine to cleave the fully extended products into shorter fragments for LC-MS/MS analysis (35, 36). Sequences of full-length extension products and relative yields were determined by LC-MS/MS analysis (Fig. 1 and Tables 4–6). The −1 frameshift products accounted for 37% of total products in a sequence with a T positioned 5′ of the 1,N⁶-ϵdA (substrate D-U, Tables 1 and 4). The fraction of extension products with a G incorporated opposite the lesion was 27% and with an A incorporated opposite the lesion was 25%. Small amounts of products with T (11%) and C (1%) incorporated were also observed in the mass spectra. The formation of the −1 frameshift products may be the result of the incoming dATP skipping the lesion and pairing with the neighboring base T (Table 4).

The T on the 5′ side of 1,N⁶-ϵdA in the template was replaced with a C, to evaluate the effect of substitution of the (5′) pyrimidine (substrate A-U, Table 1). LC-MS/MS results revealed 14 sequences of full-length products corresponding to nine peaks of M − 2H ions (Table 5). With this template, 70% of the products were due to −1 frameshifts, followed by 16% A and 14% T incorporation opposite the lesion. Extension products containing a G opposite 1,N⁶-ϵdA were not observed in this setting, presumably because the dGTP skipped 1,N⁶-ϵdA and paired with the C positioned 5′ to the lesion to yield a frameshift. Human pol η, like many other DNA polymerases (35), can also catalyze blunt-end addition of dATP or dGTP. Some extension oligonucleotides were added to the second nucleotide following the blunt end in this experiment (Table 5).

We also included a template containing 1,N⁶-ϵdA in another sequence context with a C in the 5′ position (substrate C-U, Table 1), one that had been used in a previous study of 1,N⁶-ϵdA by Levine *et al.* (34) (Table 6, Fig. 1B, supplemental Table S1). Again we found −1 frameshifts (39%, dominated by an A in the next position) and incorporation of A (29%) and G (23%) opposite 1,N⁶-ϵdA, instead of T (8%) and C (<1%), consistent with our results from the steady-state study with this sequence (Table 3 and supplemental Fig. S1).

Crystal Structures of Insertion-stage Ternary Human pol η Complexes—We determined five crystal structures of ternary hpol η-DNA·dNTP complexes with template strands containing 1,N⁶-ϵdA, three of which were trapped at the insertion stage. The resolution of these three structures varied between 2.12 and 2.26 Å (Table 7), and representative images of the quality of the final electron density are provided in Fig. 2, A–C. The first two complexes are of incoming dAMPNPP and dGMPNPP opposite 1,N⁶-ϵdA, the nucleoside triphosphates preferentially incorporated according to the steady-state kinetic data (ϵdA:dAMPNPP and ϵdA:dGMPNPP, see Tables 1–3 and 7). The structures revealed that the purine bases of incoming nucleotides adopt a staggered orientation relative to 1,N⁶-ϵdA in the *anti* conformation. This arrangement leads to extensive cross-strand stacking between the adducted base and A or G (Fig. 3). Stacking interactions between 1,N⁶-ϵdA and adenines from the incoming nucleotide and 3′-adjacent template residue appear to be slightly more favorable (Fig. 3B) compared with the structure with incoming G (Fig. 3D). In the latter, the adduct base appears to have shifted slightly into the major groove, whereas the relative positions of the base portions of incoming nucleotides relative to the template A located 3′ to the adduct are very similar in the two structures. In both, Gln-38 forms an H-bond to the sugar O4′ of 1,N⁶-ϵdA (Fig. 3). In the structure with dGMPNPP, guanine N2 and Gln-38 are also engaged in an H-bond (Fig. 3B), although this interaction is absent in the insertion-stage complex with incoming dAMPNPP (Fig. 3D). Shared properties of the two structures are the conformation of the template nucleotide situated 5′ to 1,N⁶-ϵdA, in that this T is directed away from the active site and is not engaged in a stacking interaction with the adduct (Fig. 3, A and C). Furthermore, the A:T base pair at the −1 position displays strong buckling in both complexes, with the thymine plane tilted relative to 1,N⁶-ϵdA. However, this orientation of the 3′-terminal primer nucleotide still leaves its O3′ at an optimal position to carry out a nucleophilic attack at the α-phosphate of the incoming nucleotide (AMPNPP or GMPNPP). The α- and β-phosphate groups of the latter are engaged in an electrostatically favorable interaction with Arg-61 from the hpol η finger domain.

An additional structure of an insertion stage hpol η complex was determined for incoming dTTP opposite 1,N⁶-ϵdA (ϵdA:dTTP, Tables 1 and 7). In this complex, thymine and the adduct base are coplanar, with the former in the standard *anti* configuration and the adduct flipped into the *syn* conformation (Fig. 4). Unlike the structures with incoming purine nucleoside triphosphates, the −1 base pair is devoid of buckling and the T 5′-adjacent to the adduct is now rotated into the active site and stacked on 1,N⁶-ϵdA. However, the *syn* orientation of the latter results in diminished overlap with the 3′-adjacent template A compared with the above complexes with incoming AMPNPP or GMPNPP (Figs. 3 and 4). The *syn*-1,N⁶-ϵdA:*anti*-dT base pair features virtually equidistant spacings between the (ϵdA)N₇···(H)N₃(T) and (ϵdA)N₆(H)···O₄(T) atom pairs. In the first contact, N₇ of 1,N⁶-ϵdA is an acceptor, and N₃ of T is a donor. Conversely, N₆ of 1,N⁶-ϵdA and O₄ of T are both acceptors. Rather than a clash between the two latter functionalities, the 2.8-Å separation might be indicative of protonation at N₆ of 1,N⁶-ϵdA. The pKₐ of N₆ in 1,N⁶-ϵdA is 4.1 (44, 45), and under the conditions used for crystallization (pH 5.5), the N₆ nitrogen

Template: 5'-GTTCTAGCGTGTAGG**U**AT
3'-CAAGATCGCACATCCATA(ƐdA)CTCC
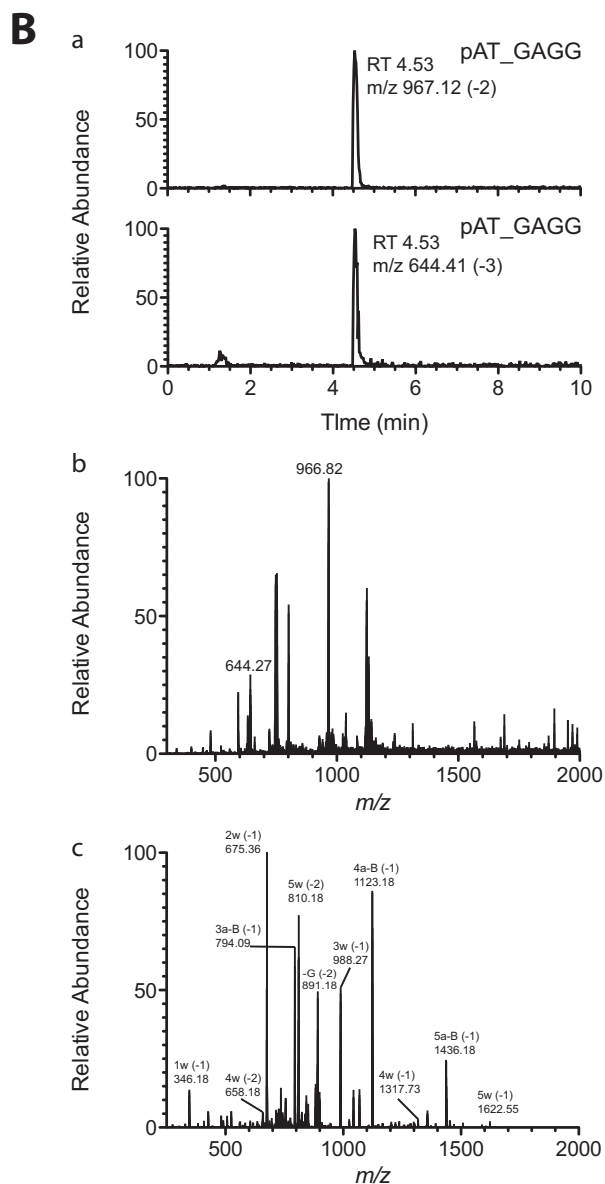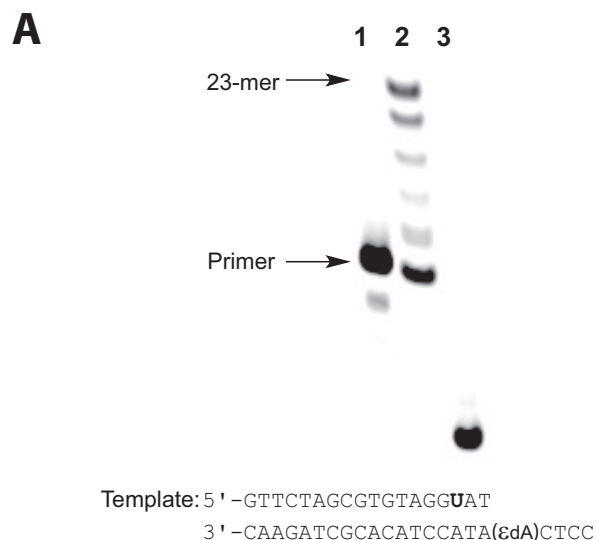
TABLE 4

LC-MS analysis of products of hpol η replication past 1,N⁶-ϵdA (T 5'-adjacent to adduct, Substrate D-U)

Products were cut at the U and begin at the CAT. An underscore represents a frameshift (deletion).

Substrate D-U 5'-(FAM)TCG TAA GCG UCA T   -3'

3'-AGC ATT CGC AGT A(ϵdA)TACT -5'

Product Sequence	m/z (-2)	m/z (-3)	Peak Area (relative units)	% Frameshifts	%A	%C	%G	%T
CAT TAT GA	1243.31	828.54	270631					11
CAT ATT GA	1247.81	831.54	581878		25			
CAT GAT GA	1255.81	836.87	638435				27	
CAT CAT GA	1235.8	823.53	12912			1		
CAT _AT GA	1091.21	727.18	493346					
CAT _TT GA	1086.7	724.13	205166					
CAT _GT GA	1099.21	732.47	167426					
CAT _CT GA	1079.2	719.13	9800	37				

of the adduct may be at least partially protonated, consistent with the geometry of the nascent base pair at the active site.

Crystal Structures of Extension-stage Ternary hpol η Complexes—Structures of ternary complexes with 1,N⁶-ϵdA opposite either primer dA or dT were determined at resolutions of 1.79 and 2.30 Å, respectively (ϵdA:dA extension and ϵdA:dT extension, Tables 1 and 7; Fig. 2, *D* and *E*). Unlike the structure of the insertion complex with dTTP opposite the adduct, the latter adopts the energetically more favorable *anti* conformation in both extension complexes (Fig. 5). This orientation results in extensive stacking within the template strand between 1,N⁶-ϵdA and the base portions of 5'- and 3'-adjacent A and T nucleotides. In this fashion, the adduct is bracketed by Watson-Crick A:T(MPNPP) pairs at the 0 and −2 positions. As in the insertion complexes, Gln-38 establishes an H-bond to the sugar O4' of the adducted nucleotide, but the Arg-61 side chain has swung away from the phosphates of the incoming nucleotide, and its guanidino moiety is directed into the major groove (Fig. 5). Similar to the dTTP insertion complex, the stacked template nucleotides include the T 5'-adjacent to Ap(1,N⁶-ϵdA) that is next in line to be replicated. The *anti* conformation of 1,N⁶-ϵdA leaves insufficient room for either dA or dT from the extended primer to be accommodated in the standard *anti* conformation (modeled nucleotides colored in *gray* in Fig. 5). Indeed, the electron density maps show good density for the phosphate group of the 3'-terminal primer nucleotide in the structures of the two extension-stage complexes but only partial density for its sugar moiety and no density even at the 0.7 σ level for the nucleobase portion (Fig. 2, *D* and *E*). The disordered state of the 3'-terminal T is consistent with the relatively low proclivity by hpol η to insert T (or A when the 5'-adjacent

FIGURE 1. **LC-MS analysis of products of extension of primer (opposite template 1,N⁶-ϵdA, substrate C-U, Table 1) by hpol η in the presence of all four dNTPs.** *A*, denaturing PAGE image showing hpol η extension across the 1,N⁶-ϵdA adduct: *lane 1*, 18-mer oligonucleotide primer containing a 5'-FAM label (from substrate C-U, Table 1); *lane 2*, TLS polymerase extension reaction with hpol η and 18-mer primer/23-mer template duplex (substrate C-U, Table 1); *lane 3*, cleavage of hpol η extension reaction products with UDG and piperidine. *B*, mass spectra of frameshift product pAT_GAGG (relative abundance of total ion current measured) (*underscore* denotes frameshift): *panel a*, LC chromatograms of product ions *m/z* 967 (−2 charge) and *m/z* 644 (−3 charge); *panel b*, mass spectrum of peak eluted at t_R 4.53 min in *panel b* (product mixture); *panel c*, CID spectrum of *m/z* 967. See supplemental Table S1 for assignments.

TABLE 5

LC-MS analysis of products of hpol η replication past template 1,N^6-εdA (C 5'-adjacent to adduct, Substrate A-U)

Products were cut at the U and begin at the 3' T. An underscore represents a frameshift (deletion). In this case the oligonucleotide pair included an upstream UT mispair. See Supplemental Data Fig. S3 for LC-MS data. The relative units differ from Tables 4 and 6 due to instrumental settings.

```
Substrate A–U  5´-(FAM)TCG TAA GCG TCU T          -3´
                   3´-AGC ATT CGC AGT A(εdA)C ACT-5´
```

Product sequence	m/z (-2)	Peak area (relative units)	% Frameshifts	%A	%C	%T
T_G TGA	798.01	935	70%			
T_G TGA A	954.62	8466				
T_G TGA G	962.62	2409				
T_G TGA C	942.60	624				
T_G TGA T	950.11	817				
T_G TGA AA	1111.22	1316				
T_G TGA AG	1119.22	200				
TAG TGA	954.62	1734		16%		
TAG TGA A	1111.22	1076				
TAG TGA G	1119.22	542				
TCG TGA	942.60	617			<1%	
TTG TGA	950.11	62				14%
TTG TGA A	1106.72	2051				
TTG TGA G	1114.71	792				

TABLE 6

LC-MS analysis of products of hpol η replication past template 1,N^6-εdA (T 5'-adjacent to adduct, Substrate C-U) (34)

Products were cut at the U and begin at the 3' AT. An underscore represents a frameshift (deletion). See Fig. 1 and Supplemental Data Table S1 for LC-MS data.

```
Substrate C–U  5´-(FAM)GTT CTA GCG TGT AGG UAT        -3´
                   3´-CAA GAT CGC ACA TCC ATA (εdA)CT CC-5´
```

Product Sequence	m/z (-2)	m/z (-3)	Peak Area (relative units)	% Frameshifts	%A	%C	%G	%T
ATT GAGG	1119.22	745.81	92506					8
ATA GAGG	1123.73	748.82	340061		29			
ATG GAGG	1131.73	754.15	268590				23	
ATC GAGG	1111.715	740.81	9427			1		
AT_ GAGG	967.12	644.41	394409					
AT_ TAGG	954.62	636.08	22783					
AT_ AAGG	959.12	639.08	29764					
AT_ CAGG	947.11	631.07	3966	39				

template nucleotide is not T) opposite the 1,N^6-εdA adduct and its preference for purines (Tables 2–6) with concomitant −1 frameshifts (Tables 4–6).

Discussion

The kinetic results presented here for insertion by hpol η at the 1,N^6-εdA adduct demonstrate that this lesion is significantly miscoding (Tables 2 and 3; supplemental Fig. S1). Under steady-state conditions, incorporation of T opposite 1,N^6-εdA is strongly attenuated relative to insertion of T opposite A, and both purines are preferred over T (Tables 2 and 3). However, all four possible insertions opposite the adduct lack a burst phase

as evidenced by our pre-steady-state analysis (supplemental Fig. S2). Therefore, it is unnecessary to invoke impediments during the extension step as the main reason for the low efficiency of bypass past the 1,N^6-εdA adduct by hpol η, and the LC-MS/MS results (Tables 4–6) are consonant with the kinetic insertion results (Tables 2 and 3).

Our misincorporation results may be compared with previous literature. Incorporation of A, C, and G opposite 1,N^6-εdA has been reported in different mammalian cell lines and extracts, in varying ratios (24, 26–28). T incorporation is reflected in a lack of mutation, but the mutagenic frequency is a function of the DNA repair status of each cell line. Pandya and co-workers (24, 27) reported a 70% mutation frequency for 1,N^6-εdA in (monkey) COS7 cells, utilizing a single-stranded vector. Of these mutations, 63% corresponded to C incorporation (*i.e.* A → G transition), 6% to A incorporation, and 1% to G incorporation. No frameshift analysis was reported. In 2000, the same laboratory (26) utilized a double-stranded vector with HeLa, HCT116, and (HEK) 293 cells, derived from human cervical cancer, colon cancer, and embryonic kidney epithelium, respectively. High percentages of large deletions were reported in the 1,N^6-εdA-plasmid cells (16–89%), with deletion of several hundred to 2000 bases. The number of targeted single mutations was low in the HTC116 cells and higher in the HeLa cells (HEK293 not reported). Of the 25 HeLa cell mutants analyzed with 1,N^6-εdA, 36% corresponded to G insertion, 16% correspond to C insertion, and 48% corresponded to A inser-

TABLE 7
Crystal data, data collection parameters, and structure refinement statistics

Complex	εdA·dTTP	εdA·dAMPNPP	εdA·dGMPNPP	εdA·dT extension	εdA·dA extension
Data collection					
Wavelength (Å)	0.97856	0.97872	0.97872	0.97856	0.97856
Space group	$P6_1$	$P6_1$	$P6_1$	$P6_1$	$P6_1$
Resolution (Å)	50–2.26 (2.30–2.26)[a]	50–2.12 (2.16–2.12)	50–2.15 (2.19–2.15)	50–2.30 (2.34–2.30)	50–1.79 (1.82–1.79)
Unit cell $a = b$, c (Å)	99.04, 81.83	99.13, 81.40	98.93, 81.71	98.42, 81.97	98.66, 82.00
Unique reflections	21,572 (1,058)	25,919 (1,305)	24,805 (1,213)	20,156 (1,004)	42,790 (2,112)
Completeness (%)	100 (99.8)	100 (100)	100 (100)	99.9 (99.9)	99.7 (99.8)
$I/\sigma(I)$	12.57 (1.70)	15.90 (1.81)	15.00 (1.70)	11.80 (1.96)	19.52 (1.83)
Wilson B-factor (Å²)	18.5	26.7	25.7	15.1	17.6
R-merge	0.165 (0.893)	0.135 (0.921)	0.136 (0.996)	0.169 (0.879)	0.102 (0.902)
Redundancy	7.3 (5.1)	7.6 (7.2)	7.6 (7.4)	5.6 (5.1)	7.5 (7.3)
Refinement					
R-work	0.156 (0.196)	0.175 (0.200)	0.170 (0.221)	0.156 (0.197)	0.164 (0.204)
R-free	0.212 (0.285)	0.239 (0.271)	0.223 (0.296)	0.233 (0.295)	0.212 (0.260)
No. of atoms protein/DNA	3,387/390	3,395/390	3,397/390	3,367/374	3,429/374
dNMPNPP/Mg²⁺	29/2 (Ca²⁺)	30/2	31/2	29/2	29/2
Water/solute	351/1	308/3	343/1	332/0	532/2
Protein residues	434	436	436	431	447
B-factor (Å²)					
Average	29.7	35.1	33.9	27.4	23.7
Protein/DNA	28.9/33.4	34.3/37.7	32.9/38.5	26.3/33.9	21.7/28.5
dNMPNPP/Mg²⁺	20.6/20.1	29.8/28.6	38.3/36.3	16.6/14.5	12.4/10.1
Water/glycerol	34.1/25.0	39.7/36.9	38.1/22.0	31.4/ -	32.5/21.5
Root mean square deviations					
Bonds (Å)	0.010	0.009	0.009	0.008	0.011
Angles (degree)	1.2	1.1	1.2	1.1	1.1
Ramachandran					
Favored (%)	97	97	97	97	98
Allowed (%)	3	2.5	2.8	2.5	1.5
Outliers (%)	0	0.5	0.2	0.5	0.5
Protein Data Band code	5DG7	5DG8	5DG9	5DGA	5DGB

[a] Statistics for the highest resolution shell are shown in parentheses.

tion. One- and two-base frameshifts were not reported. In 2008 Tolentino *et al.* (28) used a double-stranded vector containing 1,N⁶-εdA with extracts of HeLa cells and XPV cells. The misincorporation frequency was very low, and with the HeLa cells only 2–3 mutants were seen for A, G, and C insertion, making any conclusions about preferences untenable.

At the time that some of the previous cellular mutation results were reported (24, 26, 27), the repair of 1,N⁶-εdA by glycosylases (46, 47) was known but repair by AlkB (25) and its mammalian orthologs was not recognized yet. The compositions of the DNA polymerase pools in these cell lines are largely uncharacterized, and the assignment of actions of the individual polymerases is not possible based on that information. As Levine *et al.* (26) state in comparing their results with cells of human origin with (monkey) COS7 cells (24): "...there are several differences in the design of these two studies, including single-stranded *versus* double-stranded vector, sequence context, location of the DNA adduct relative to replication origin, and host cells. One or several of these factors could have contributed to the differences observed." Ultimately, the contribution of hpol η to mutations should be evaluated in cells equivalent in all respects except hpol η (and the characterization of other DNA polymerases and repair enzymes established).

Our results with several sequences, including that used by Levine *et al.* (34), clearly show that hpol η bypasses 1,N⁶-εdA in a highly error-prone manner, dominated by purine incorporations or generation of −1 frameshifts instead of insertion of T. This conclusion is based on both the kinetic analyses (Tables 2 and 3; supplemental Fig. S1) and LC-MS/MS analysis of the extended products (Tables 4–6), including sequences used previously by others (substrate C, Table 1) (34). These misin-

corporation patterns are also consistent with the results obtained in mammalian cells (26–28), although there is considerable variation among cell lines (26). Although A, C, and G insertions have all been reported opposite 1,N⁶-εdA in many systems, the presence of frameshifts in cells replicating past 1,N⁶-εdA has not been addressed. Levine *et al.* (26) listed a −1 deletion probe to be used for detecting frameshifts in cells but did not report any analyses for such events. In that study, large deletions (several hundred to 2000 bp) were observed in 16–89% of the mutants, depending on the cell line (26).

We found that the higher rate of incorporation of purine nucleoside triphosphates is in large part dependent on the availability of the matching template nucleotide 5'-adjacent to 1,N⁶-εdA (*i.e.* T and C for incoming dATP and dGTP, respectively). This purine incorporation is related in part to −1 frameshifts (Tables 4–6). The structures of insertion-stage complexes with incoming non-hydrolyzable dNTP analogs (dAMPNPP and dGMPNPP) in the presence of Mg²⁺ reveal that the 1,N⁶-εdA and adenine (guanine) bases are offset at the active site and, instead of direct pairing, engaged in stacking interactions across the template and primer strands (Fig. 3). Thus, unlike the structures of isolated oligonucleotide duplexes (30, 31), where the adduct switches into a *syn* orientation to accommodate pairing with a purine, 1,N⁶-εdA remains in the favored *anti* orientation and the incoming purines adopt the observed staggered orientation.

From the states seen in the two insertion-stage complex structures, the replication process can proceed in two distinct ways. (i) The incoming purine is accommodated opposite the adduct (Tables 4 and 6). (ii) Alternatively, the template T(C) 5'-adjacent to the adduct, seen outside the active site in the
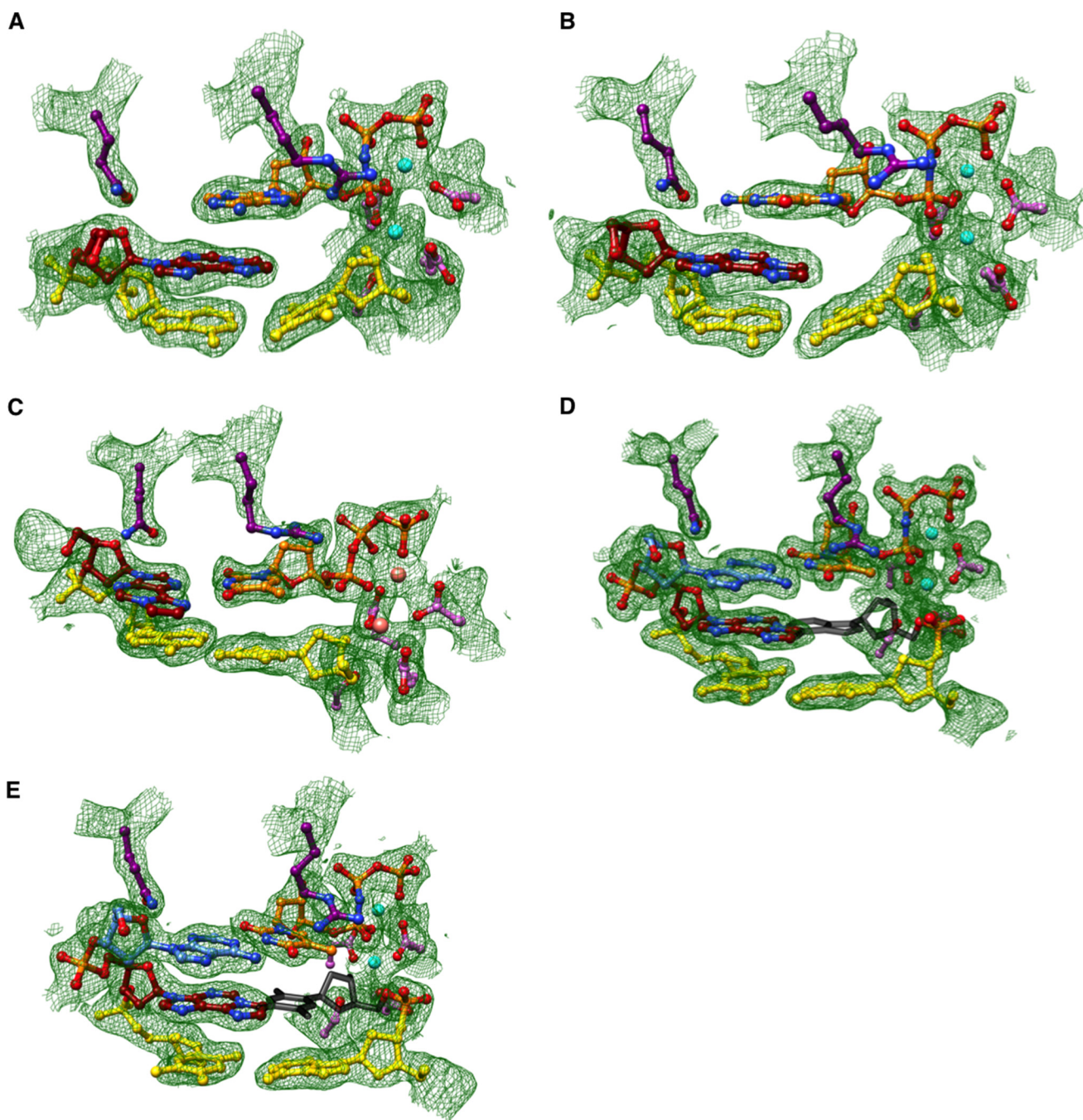
FIGURE 2. **Quality of the final models of ternary hpol η complexes with 1,N^6-εdA-adducted DNA template strands.** Fourier ($2F_o - F_c$) sum electron density drawn at the 1σ threshold (*green meshwork*) around the active site region. *A*, staggered arrangement of dAMPNPP and 1,N^6-εdA; insertion stage (εdA: dAMPNPP, Tables 1 and 7). *B*, staggered arrangement of dGMPNPP and 1,N^6-εdA; insertion stage (εdA:dGMPNPP, Tables 1 and 7). *C*, dTTP opposite *syn* 1,N^6-εdA; insertion stage (εdA:dTTP, Tables 1 and 7). *D*, *anti* 1,N^6-εdA opposite conformationally disordered primer dA, followed by dTMPNPP opposite template dA; extension stage (εdA:dA extension, Tables 1 and 7). *E*, *anti* 1,N^6-εdA opposite conformationally disordered primer dT, followed by dTMPNPP opposite template dA; extension stage (εdA:dT extension, Tables 1 and 7). Selected active site residues are colored by atom with carbon atoms shown in *maroon* (1,N^6-εdA), *orange* (incoming nucleotide), *light blue* (template nucleotide 5'-adjacent to 1,N^6-εdA; *D* and *E*), *purple* (Arg-61 and Gln-38 from the finger domain), or *magenta* (Asp/Glu coordinating to Mg^{2+} or Ca^{2+}). Base pairs at the −1 (*A–C*) or −2 (*D* and *E*) positions are shown in *yellow*, primer dA and dT in idealized stacked positions (that would result in a clash with *anti* 1,N^6-εdA) in *D* and *E*, respectively, are shown in *dark gray*, and Mg^{2+} and Ca^{2+} ions are *cyan* and *pink spheres*, respectively.

structures (Fig. 3), rotates inward and above the adduct and then pairs with dAMPNPP (dGMPNPP), thus resulting in the −1 frameshift products that constituted the majority of the extended oligonucleotides according to the LC-MS/MS analysis. The actual configurations by which A or G are accommodated opposite 1,N^6-εdA in the template·primer duplex remain

unclear from the two structures at the insertion stage, although it is possible that the adduct and purine nucleotides are stacked in a cross-strand fashion.

The structure of the extension complex with dA opposite 1,N^6-εdA is useful in addressing this question. Rather than in the staggered configuration, the 1,N^6-εdA:A pair is wedged

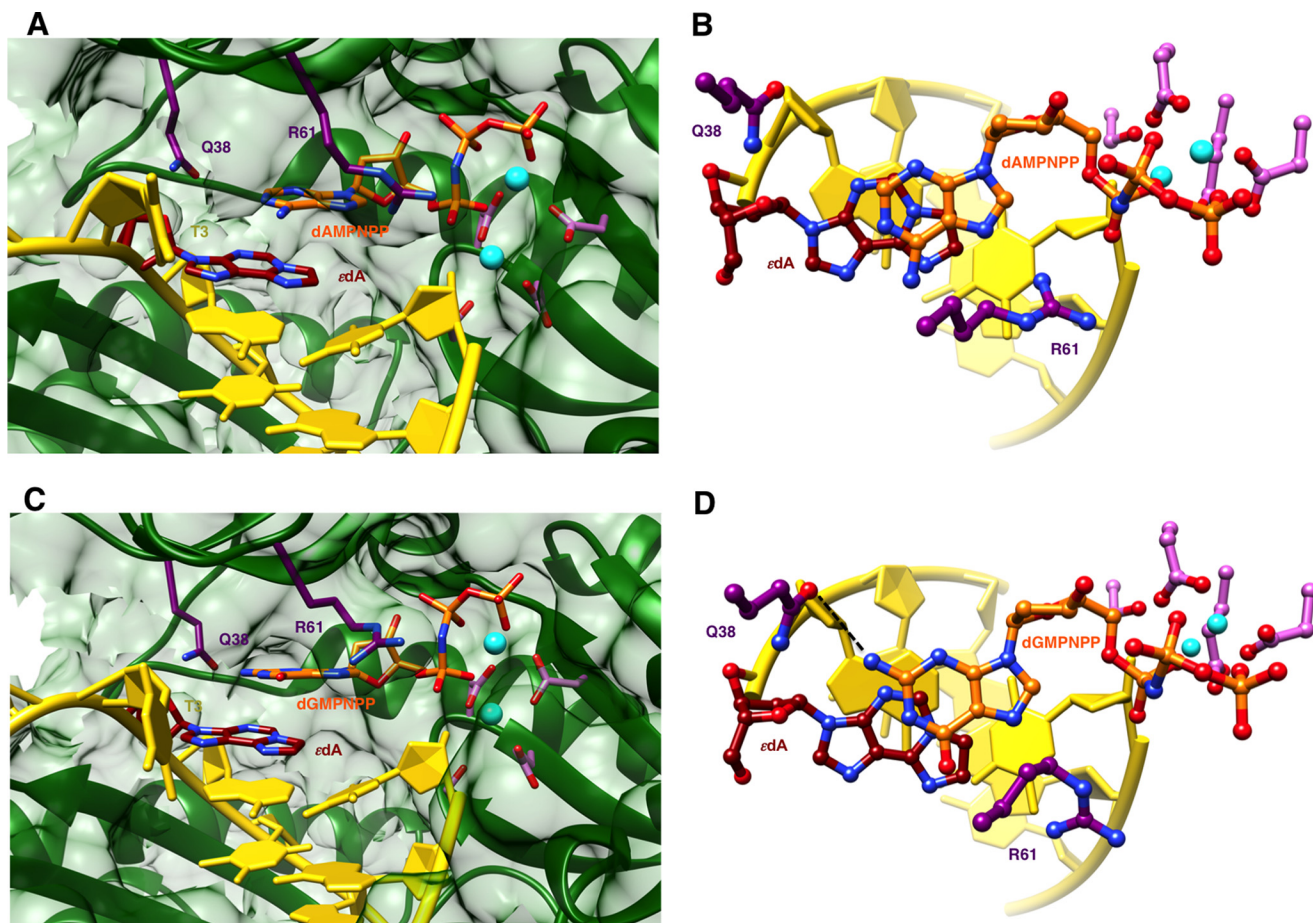FIGURE 3. **Staggered arrangements of incoming purine nucleoside triphosphates and 1,N⁶-εdA in two hpol η insertion stage complexes.** *A,* active site conformation in the complex with dAMPNPP opposite 1,N⁶-εdA, viewed into the DNA major groove; *B,* rotated by 90° and viewed perpendicular to the adenine plane (εdA:dAMPNPP, Tables 1 and 7). *C,* active site conformation in the complex with dGMPNPP opposite 1,N⁶-εdA, viewed into the DNA major groove; and *D,* rotated by 90° and viewed perpendicular to the guanine plane (εdA:dGMPNPP, Tables 1 and 7). Selected active site residues are colored by atom with carbon atoms shown in *maroon* (1,N⁶-εdA), *orange* (incoming nucleotide), *purple* (Arg-61 and Gln-38 from the finger domain), or *magenta* (Asp/Glu coordinating to Mg^{2+}; *cyan spheres*).
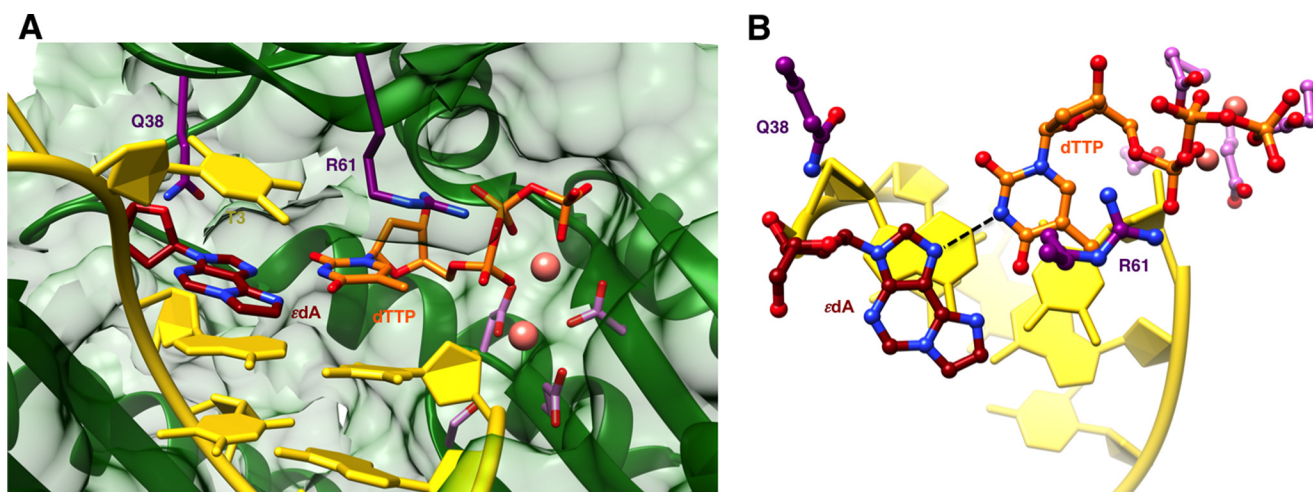

FIGURE 4. **Active site conformation in the ternary hpol η insertion step complex with dTTP opposite 1,N⁶-εdA.** *A,* view into the DNA major groove; *B,* rotated by 90° and viewed perpendicular to the thymine and adduct base planes (εdA:dTTP, Tables 1 and 7). Selected active site residues are colored by atom with carbon atoms shown in *maroon* (1,N⁶-εdA), *orange* (incoming dTTP), *purple* (Arg-61 and Gln-38 from the finger domain), or *magenta* (Asp/Glu coordinating to Ca^{2+}; *pink spheres*).

between A:T(TP) pairs at the −2 and 0 positions that are separated by ∼7 Å in an axial direction (Fig. 5, *A* and *C*). The staggered orientation following insertion can thus be discarded, but

the nucleobase portion of primer dA is completely disordered, suggesting a position of the adduct partner either inside the major or the minor groove.
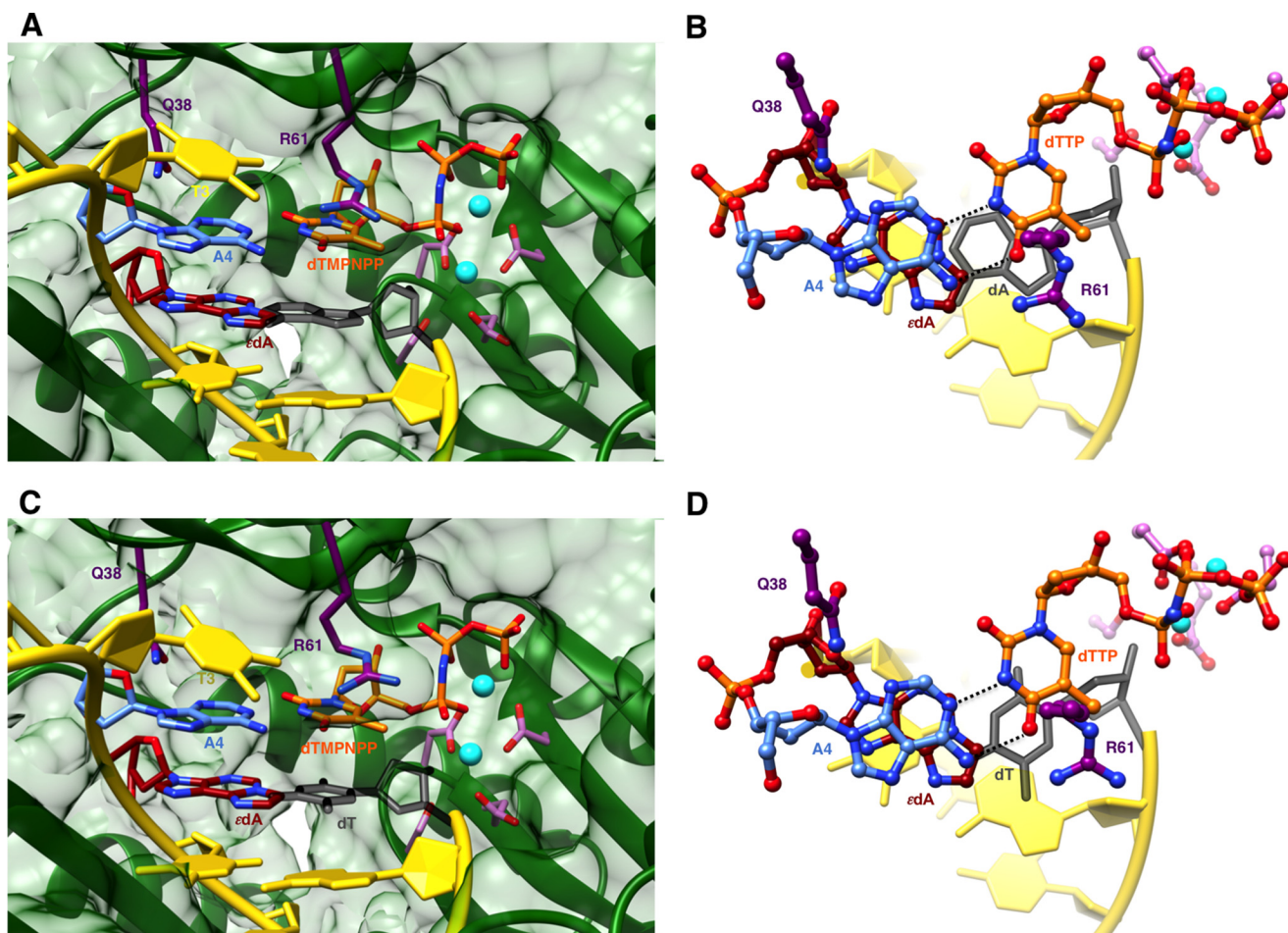
FIGURE 5. **Active site conformations in two ternary hpol η extension step complexes with primer dA or dT opposite 1,N⁶-εdA, followed by dTMPNPP across template dA.** *A*, ternary extension stage complex with dA opposite 1,N⁶-εdA, viewed into the major groove, and *B*, rotated by 90° and viewed perpendicular to the best plane through the nascent base pair (εdA:dA extension, Tables 1 and 7). *C*, ternary extension stage complex with dT opposite 1,N⁶-εdA viewed into the major groove; *D*, rotated by 90° and viewed perpendicular to the best plane through the nascent base pair (εdA:dT extension, Tables 1 and 7). The 3'-terminal primer nucleoside (dA/dT) is disordered in both complexes. Residues shown with *dark gray* bonds represent idealized stacked positions of primer dA (*A* and *B*) and primer dT (*C* and *D*). The conformational disorder of these residues in the two complex structures might arise from a clash between dA or dT in the modeled orientation with *anti* 1,N⁶-εdA. Selected active site residues are colored by atom with carbon atoms shown in *maroon* (1,N⁶-εdA), *orange* (incoming nucleotide), *light blue* (template nucleotide 5'-adjacent to 1,N⁶-εdA), *purple* (Arg-61 and Gln-38 from the finger domain), or *magenta* (Asp/Glu coordinating to Mg²⁺; *cyan spheres*).

Even the smaller thymine moiety of dT is disordered in the second extension-stage complex (Fig. 5, *C* and *D*). However, the *anti* orientation of 1,N⁶-εdA is common to both complexes and is likely preferred because it allows for more optimal stacking interactions with flanking bases, even if it results in a suboptimal arrangement of the pairing partner and loss of H-bonds. This conclusion is supported by the structural and kinetic data for T incorporation opposite 1,N⁶-εdA. The structure of the corresponding insertion complex shows the adduct in the *syn* conformation and therefore has diminished stacking with the 3'-adjacent template base (*A*; Fig. 5). The incoming T and 1,N⁶-εdA are in the same plane, and it is possible, based on the relative orientation and taking into account pK_a data for the adduct and the acidic pH of the crystallization solution, that two H-bonds are established between the pairing partners. However, the 1000-fold lower efficiency of T incorporation opposite 1,N⁶-εdA relative to T opposite A (steady-state results, Table 2) renders it unnecessary to envision an optimal structural context for the 1,N⁶-εdA:T pair at the insertion step. Moreover, the incoming C can form a bifurcated H-bond with its N4 amino group to the

N6 and N7 acceptors of the adduct or, alternatively (envisioning a protonated state of C (pK_a 4.6) under pH 5.5 crystallization conditions), two H-bonds. However, these assumptions are mute as the efficiency of C incorporation is further reduced compared with T (4-fold) and considerably below the levels of efficiency for A or G incorporation and frameshifting.

The structures of incoming dAMPNPP and dGMPNPP in a staggered orientation relative to 1,N⁶-εdA and the kinetic data manifesting preferred incorporation of purines opposite the adduct, accompanied with frameshifts offer some parallels to our observations of hpol η-catalyzed bypass reactions opposite an abasic site. Specifically, we invoke a "purine rule," meaning that dATP and dGTP are preferred over dCTP and dTTP by this polymerase opposite an abasic lesion (48). Structures of the preferred dNTPs opposite the abasic site in ternary hpol η complexes offered insight into this preference, in that the longer purine bases could be linked to the phosphate group of the abasic residue via water bridges. By comparison, the smaller pyrimidines were at a disadvantage, both because of the reduced level of stacking interactions and the inability to tether

them to the template strand via solvent molecules in the active site. Similarly, purines opposite the $1,N^6$-εdA adduct at the hpol η active site exploit cross-strand stacking interactions that result in facilitated error-prone bypass. In addition, at least in the case of incoming dGMPNPP, the side chain of Gln-38 mediates an interaction between guanine (N2) and the backbone of the template strand (sugar ring of the adduct, Fig. 3, *C* and *D*). Finally, the structure of the third insertion-stage complex with dTTP opposite $1,N^6$-εdA and with the adduct adopting a *syn* orientation (Fig. 5) is reminiscent of the pairing between this lesion and incoming dTTP observed in the crystal structure of a ternary hpol ι complex (49). However, this Y-family pol is more efficient and less error prone than hpol η in regard to bypass of $1,N^6$-εdA and incorporates a T opposite the lesion with only about 10-fold reduced efficiency relative to T opposite A, consistent with a more narrow active site that forces base pairs into the normally less favorable Hoogsteen configuration.

In summary, bypass of the $1,N^6$-εdA lesion by hpol η proceeds with relatively low efficiency and in an error-prone fashion by misinsertion of A and G or generation of −1 frameshifts. Thus, the outcomes of hpol η-catalyzed bypass of the bulky $1,N^6$-εdA lesion and an abasic site (48) are surprisingly similar.

Experimental Procedures

Materials—The catalytic core (amino acids 1–432) of hpol η was expressed and purified as described previously (50). Unlabeled dNTPs, T4 polynucleotide kinase, and UDG were purchased from New England Biolabs (Ipswich, MA). A mixture of four dNTPs was purchased from Invitrogen. All non-hydrolyzable dNMPNPPs were obtained from Jena Bioscience (Jena, Germany). $[\gamma\text{-}^{32}P]$ATP (specific activity 3000 Ci/mmol) was purchased from PerkinElmer Life Sciences. Biospin columns were purchased from Bio-Rad. All oligonucleotides (purified by HPLC by the manufacturers) were obtained from Midland Certified Reagent Co. (Midland, TX), Integrated DNA Technologies (Coralville, IA), or TriLink Biotechnologies (San Diego). The oligonucleotides containing $1,N^6$-εdA were from TriLink.

Steady-state Kinetics—A 13-mer primer was 5′-5/6-carboxyfluorescein (FAM)-labeled and annealed to an 18-mer template at a 1:1.2 molar ratio (Table 1). The same procedure was used for the 18/23-mer pair, annealing the primer and template in a 1:1 molar ratio. Enzyme concentrations and reaction times were optimized using time course assays to ensure ≤20% conversion of substrate to product. A typical assay solution included 4–55 nM hpol η, 5 μM primer·template duplex, 40 mM Tris-HCl buffer (pH 7.5), 5 mM MgCl₂, 10 mM DTT, 100 mM KCl, 5% glycerol (v/v), 100 μg/ml bovine serum albumin, and varying concentrations of a single dNTP (0–2 mM). Reactions were incubated at 37 °C for 5–20 min and were terminated with 9 volumes of a quench solution (20 mM EDTA, 95% formamide (v/v), bromphenol blue, and xylene cyanol). Products were resolved by electrophoresis on 18% (w/v) polyacrylamide gels containing 7.5 M urea. The gels were scanned by a Typhoon Scanner (GE Healthcare) and quantified by fluorescence intensity using ImageJ software (National Institutes of Health). Data were fit to the Michaelis-Menten equation using Prism software (GraphPad, La Jolla, CA) to estimate k_{cat} and K_m values (non-linear regression).

Pre-steady-state Kinetics—Rapid quench experiments were performed using a model RQF-3 KinTek quench flow apparatus (KinTek, Austin, TX). The 13-mer primer was ^{32}P-labeled at the 5′ end by T4 polynucleotide kinase/$[\gamma\text{-}^{32}P]$ATP and annealed to the 18-mer templates. Reactions were initiated by rapid mixing of ^{32}P-primer·template/polymerase mixtures with dNTP and Mg²⁺ at 37 °C. The final concentrations of the reactants were 50 nM hpol η, 500 nM ^{32}P-labeled primer·template complex, and 0.5 mM dNTP. Other reaction conditions are the same as described for steady-state kinetics. Reactions were quenched with 0.5 M EDTA at times varying from 5 ms to 5 s. Products were separated on 18% (w/v) polyacrylamide gels and scanned and quantitated using a PhosphorImaging system (Bio-Rad, Molecular Imager FX) and Quantity One software as described previously (35).

LC-MS/MS Analysis of Full-length Extended Products—A 5′-FAM-labeled primer containing an appropriately positioned deoxyuridine (dU) (opposite A in some but not all cases) (Table 1) was annealed to the 18- or 23-mer templates at a 1:1 molar ratio. Reaction conditions were similar to those used in steady-state kinetics assays, except that the final concentrations were 3 μM hpol η and 25 μM primer·template duplex, in a total volume of 80 μl. Reactions were initiated by addition of a mixture of 1 mM each of dNTPs (A, G, C, and T) and terminated by spin-column separation to remove dNTP and Mg²⁺ after 1 h of incubation (37 °C). The resulting products were treated with 50 units of UDG and 0.25 M hot piperidine, following a previous protocol (35, 36). The extent of the reaction was monitored by denaturing PAGE (Fig. 1A) prior to LC-MS analysis. The cleavage solution was lyophilized and reconstituted in 60 μl of H₂O.

LC-MS/MS analysis was performed on an Acquity ultraperformance liquid chromatography (UPLC) system (Waters Associates) coupled to a Thermo Finnigan LTQ mass spectrometer (Thermo Scientific, San Jose, CA) with an electrospray ionization source. Samples were separated on an Acquity UPLC BEH octadecylsilane (C18) column (1.7 μm, 2.1 × 100 mm) at a flow rate of 0.3 ml/min. The column temperature was maintained at 50 °C. Eluent A contained 10 mM NH₄CH₃CO₂ in 98% H₂O, 2% CH₃CN (v/v), and eluent B consisted of 10 mM NH₄CH₃CO₂ in 90% CH₃CN, 10% H₂O (v/v). A gradient program was run as follows: 0–3% B over 3 min, 3–20% B over 2 min, 20–100% B over 1 min, held at 100% B for 2 min, 100–0% B over 2 min, and held at 0% B for 3 min (all v/v). MS data were acquired in the negative mode and controlled by Xcalibur 2.1 software (Thermo). Electrospray ionization settings were as follows: source voltage 4 kV, source current 100 A, capillary voltage −49 V, capillary temperature 350, tube lens voltage −90 V. The most abundant species (−2 or −3 charged) were fragmented in the ion trap by collision-induced dissociation (CID) with a normalized collision energy of 35%. An activation Q of 0.25 and activation time of 30 ms were used. Oligonucleotide sequences can be identified by comparing the observed CID spectra and theoretical spectra of candidate oligonucleotide sequences calculated using Mongo Oligo Calculator 2.0 software (University of Utah, Salt Lake City). The relative yields of various DNA extension products were based on their respective peak areas in the extracted ion chromatograms.

Human pol η and 1,N⁶-Ethenodeoxyadenosine

Crystallization—Crystals were obtained by the hanging drop vapor diffusion technique at 18 °C. 1,N^6-εdA-modified DNA templates and primer sequences used in the crystallization experiments are listed in Table 1. DNA solutions were prepared by mixing template and primer strands in a 1:1 molar ratio and annealing the mixture in the presence of 10 mM sodium HEPES buffer (pH 8.0), 0.1 mM EDTA, and 50 mM NaCl at 85 °C for 10 min, followed by slow cooling to room temperature. hpol η protein was mixed with the DNA duplex in a 1:1.2 molar ratio in the presence of 50 mM Tris-HCl (pH 7.5) containing 450 mM KCl and 3 mM DTT, followed by addition of either 5 μl of 100 mM $MgCl_2$ or 5 μl of 100 mM $CaCl_2$. Using a spin concentrator with an Amicon cutoff filter (Millipore, Billerica, MA), the complex was concentrated to a final concentration of ~2 mg of protein/ml. Either dTTP or one of the non-hydrolyzable nucleoside triphosphate analogs was added to the concentrated mixtures containing Ca^{2+} or Mg^{2+}. The ternary complex solution was mixed with an equal volume of reservoir solution containing 0.10 M sodium MES (pH 5.5), 5 mM $MgCl_2$, and 16–21% (w/v) PEG 2000 monomethyl ether and equilibrated against 500-μl reservoir solutions. Crystals typically appeared after overnight incubation and were allowed to grow for 1 week. They were transferred to cryoprotectant solution containing reservoir solution along with 25% glycerol (v/v) and then frozen in liquid nitrogen for data collection.

X-ray Diffraction Data Collection, Structure Determination, and Refinement—X-ray diffraction data were collected at 100 K either on the 21-ID-F or the 21-ID-G beamline of the Life Sciences Collaborative Access Team at the Advanced Photon Source, Argonne National Laboratory (Argonne, IL). All data were processed with the program HKL2000 (51). (Data collection statistics are summarized in Table 7.) All structures were determined by molecular replacement in MOLREP (52, 53), using the coordinates of the complex between hpol η and native DNA (Protein Data Bank code 4O3N) as the search model. Structures were refined using PHENIX (54), and model building was carried out in COOT (55). Model statistics and geometric parameters are summarized in Table 7. Illustrations were generated with the program UCSF Chimera (56).

Author Contributions—A. P. crystallized the protein complexes and solved the structures; Q. Z. was responsible for the pre-steady-state and part of the steady-state kinetic analysis and part of the LC-MS measurements; Y. S. purified the enzyme and carried out part of the steady-state kinetic analysis and preparation of extended primers for some of the extended primers for LC-MS analysis; K. M. J. did part of the LC-MS measurements, and F. P. G. and M. E. conceived the studies and wrote the paper, along with Y. S.

References

1. Friedberg, E. C., Walker, G. C., Siede, W., Wood, R. D., Schultz, R. A., and Ellenberger, T. (2006) *DNA Repair and Mutagenesis.* 2nd Ed., American Society for Microbiology, Washington, D. C.
2. Shigenaga, M. K., Hagen, T. M., and Ames, B. N. (1994) Oxidative damage and mitochondrial decay in aging. *Proc. Natl. Acad. Sci. U.S.A.* **91,** 10771–10778
3. McCann, J., Choi, E., Yamasaki, E., and Ames, B. N. (1975) Detection of carcinogens as mutagens in the *Salmonella*/microsome test: assay of 300 chemicals. *Proc. Natl. Acad. Sci. U.S.A.* **72,** 5135–5139
4. Erickson, R. P. (2003) Somatic gene mutation and human disease other than cancer. *Mutat. Res.* **543,** 125–136
5. Weismann, C. G., and Gelb, B. D. (2007) The genetics of congenital heart disease: a review of recent developments. *Curr. Opin. Cardiol.* **22,** 200–206
6. Wessels, M. W., and Willems, P. J. (2010) Genetic factors in non-syndromic congenital heart malformations. *Clin. Genet.* **78,** 103–123
7. Malaveille, C., Bartsch, H., Barbin, A., Camus, A. M., Montesano, R., Croisy, A., and Jacquignon, P. (1975) Mutagenicity of vinyl chloride, chloroethylene oxide, chloroacetaldehyde and chloroethanol. *Biochem. Biophys. Res. Commun.* **63,** 363–370
8. DeMott, M. S., and Dedon, P. C. (2010) in *The Chemical Biology of DNA Damage* (Geacintov, N. E., and Broyde, S., eds) pp. 21–51, Wiley-VCH Verlag GmbH, KGaA Weinheim, Germany
9. Swenberg, J. A., Lu, K., Moeller, B. C., Gao, L., Upton, P. B., Nakamura, J., and Starr, T. B. (2011) Endogenous versus exogenous DNA adducts: their role in carcinogenesis, epidemiology, and risk assessment. *Toxicol. Sci.* **120,** S130–S145
10. Leonard, N. J. (1992) Etheno-bridged nucleotides in structural diagnosis and carcinogenesis. *Chemtracts-Biochem. Mol. Biol.* **3,** 273–297
11. Dudock, B. S., Katz, G., Taylor, E. K., and Holley, R. W. (1969) Primary structure of wheat germ phenylalanine transfer RNA. *Proc. Natl. Acad. Sci. U.S.A.* **62,** 941–945
12. Sattsangi, P. D., Leonard, N. J., and Frihart, C. R. (1977) 1,N^2-Ethenoguanine and N^2,3-ethenoguanine. Synthesis and comparison of the electronic spectral properties of these linear and angular triheterocycles related to the Y bases. *J. Org. Chem.* **42,** 3292–3296
13. Secrist, J. A., 3rd., Barrio, J. R., Leonard, N. J., and Weber, G. (1972) Fluorescent modification of adenosine-containing coenzymes. Biological activities and spectroscopic properties. *Biochemistry* **11,** 3499–3506
14. Leonard, N. J. (1984) Etheno-substituted nucleotides and coenzymes: fluorescence and biological activity. *CRC Crit. Rev. Biochem.* **15,** 125–199
15. Leonard, N. J. (1993) Etheno-bridged nucleotides in enzyme reactions and protein binding. *Chemtracts-Biochem. Mol. Biol.* **4,** 251–284
16. Barbin, A., Brésil, H., Croisy, A., Jacquignon, P., Malaveille, C., Montesano, R., and Bartsch, H. (1975) Liver-microsome-mediated formation of alkylating agents from vinyl bromide and vinyl chloride. *Biochem. Biophys. Res. Commun.* **67,** 596–603
17. Laib, R. J., Gwinner, L. M., and Bolt, H. M. (1981) DNA alkylation by vinyl chloride metabolites: etheno derivatives or 7-alkylation of guanine? *Chem. Biol. Interact.* **37,** 219–231
18. Fedtke, N., Boucheron, J. A., Walker, V. E., and Swenberg, J. A. (1990) Vinyl chloride-induced DNA adducts. II. Formation and persistence of 7-(2′-oxoethyl)guanine and N^2,3-ethenoguanine in rat tissue DNA. *Carcinogenesis* **11,** 1287–1292
19. Rindgen, D., Nakajima, M., Wehrli, S., Xu, K., and Blair, I. A. (1999) Covalent modifications to 2′-deoxyguanosine by 4-oxo-2-nonenal, a novel product of lipid peroxidation. *Chem. Res. Toxicol.* **12,** 1195–1204
20. Carvalho, V. M., Asahara, F., Mascio, P. D., de Arruda Campos, I. P., Cadet, J., and Medeiros, M. H. (2000) Novel 1,N^6-etheno-2′-deoxyadenosine adducts from lipid peroxidation products. *Chem. Res. Toxicol.* **13,** 397–405
21. Guengerich, F. P., and Raney, V. M. (1992) Formation of etheno adducts of adenosine and cytidine from 1-halooxiranes. Evidence for a mechanism involving initial reaction with the endocyclic nitrogens. *J. Am. Chem. Soc.* **114,** 1074–1080
22. Swenberg, J. A., Fedtke, N., Ciroussel, F., Barbin, A., and Bartsch, H. (1992) Etheno adducts formed in DNA of vinyl chloride-exposed rats are highly

persistent in liver. *Carcinogenesis* **13,** 727–729

23. Basu, A. K., Niedernhofer, L. J., and Essigmann, J. M. (1987) Deoxyhexanucleotide containing a vinyl chloride induced DNA lesion, 1,*N⁶*-ethenoadenine: synthesis, physical characterization, and incorporation into a duplex bacteriophage M13 genome as part of an *amber* codon. *Biochemistry* **26,** 5626–5635

24. Pandya, G. A., and Moriya, M. (1996) 1,*N⁶*-Ethenodeoxyadenosine, a DNA adduct highly mutagenic in mammalian cells. *Biochemistry* **35,** 11487–11492

25. Delaney, J. C., Smeester, L., Wong, C., Frick, L. E., Taghizadeh, K., Wishnok, J. S., Drennan, C. L., Samson, L. D., and Essigmann, J. M. (2005) AlkB reverses etheno DNA lesions caused by lipid oxidation *in vitro* and *in vivo*. *Nat. Struct. Mol. Biol.* **12,** 855–860

26. Levine, R. L., Yang, I.-Y., Hossain, M., Pandya, G. A., Grollman, A. P., and Moriya, M. (2000) Mutagenesis induced by a single 1,*N⁶*-ethenodeoxyadenosine adduct in human cells. *Cancer Res.* **60,** 4098–4104

27. Moriya, M., Pandya, G. A., Johnson, F., and Grollman, A. P. (1999) in *Exocyclic DNA Adducts in Mutagenesis and Carcinogenesis* (Singer, B., and Bartsch, H., eds) IARC Sci. Publication No. 150, pp. 263–270, Int. Agency Res. Cancer Scientific Publications, Lyon, France

28. Tolentino, J. H., Burke, T. J., Mukhopadhyay, S., McGregor, W. G., and Basu, A. K. (2008) Inhibition of DNA replication fork progression and mutagenic potential of 1,*N⁶*-ethenoadenine and 8-oxoguanine in human cell extracts. *Nucleic Acids Res.* **36,** 1300–1308

29. Kouchakdjian, M., Eisenberg, M., Yarema, K., Basu, A., Essigmann, J., and Patel, D. J. (1991) NMR studies of the exocyclic 1,*N⁶*-ethenodeoxyadenosine adduct (εdA) opposite thymidine in a DNA duplex. Nonplanar alignment of εdA(*anti*) and dT(*anti*) at the lesion site. *Biochemistry* **30,** 1820–1828

30. de los Santos, C., Kouchakdjian, M., Yarema, K., Basu, A., Essigmann, J., and Patel, D. J. (1991) NMR studies of the exocyclic 1,*N⁶*-ethenodeoxyadenosine adduct (εdA) opposite deoxyguanosine in a DNA duplex. εdA(*syn*)·dG(*anti*) pairing at the lesion site. *Biochemistry* **30,** 1828–1835

31. Leonard, G. A., McAuley-Hecht, K. E., Gibson, N. J., Brown, T., Watson, W. P., and Hunter, W. N. (1994) Guanine-1,*N⁶*-ethenoadenine base pairs in the crystal structure of d(CGCGAATT(εdA)GCG). *Biochemistry* **33,** 4755–4761

32. Singer, B., Abbott, L. G., and Spengler, S. J. (1984) Assessment of mutagenic efficiency of two carcinogen-modified nucleosides, 1,*N⁶*-ethenodeoxyadenosine and *O⁴*-methyldeoxythymidine, using polymerases of varying fidelity. *Carcinogenesis* **5,** 1165–1171

33. Calabretta, A., and Leumann, C. J. (2013) Base pairing and miscoding properties of 1,*N⁶*-ethenoadenine- and 3,*N⁴*-ethenocytosine-containing RNA oligonucleotides. *Biochemistry* **52,** 1990–1997

34. Levine, R. L., Miller, H., Grollman, A., Ohashi, E., Ohmori, H., Masutani, C., Hanaoka, F., and Moriya, M. (2001) Translesion DNA synthesis catalyzed by human pol η and pol κ across 1,*N⁶*-ethenodeoxyadenosine. *J. Biol. Chem.* **276,** 18717–18721

35. Zang, H., Goodenough, A. K., Choi, J. Y., Irimia, A., Loukachevitch, L. V., Kozekov, I. D., Angel, K. C., Rizzo, C. J., Egli, M., and Guengerich, F. P. (2005) DNA adduct bypass polymerization by *Sulfolobus solfataricus* DNA polymerase Dpo4: analysis and crystal structures of multiple base pair substitution and frameshift products with the adduct 1,*N²*-ethenoguanine. *J. Biol. Chem.* **280,** 29750–29764

36. Christov, P. P., Angel, K. C., Guengerich, F. P., and Rizzo, C. J. (2009) Replication past the *N⁵*-methyl-formamidopyrimidine lesion of deoxyguanosine by DNA polymerases and an improved procedure for sequence analysis of *in vitro* bypass products by mass spectrometry. *Chem. Res. Toxicol.* **22,** 1086–1095

37. Choi, J. Y., Chowdhury, G., Zang, H., Angel, K. C., Vu, C. C., Peterson, L. A., and Guengerich, F. P. (2006) Translesion synthesis across *O⁶*-alkylguanine DNA adducts by recombinant human DNA polymerases. *J. Biol. Chem.* **281,** 38244–38256

38. Eoff, R. L., Irimia, A., Egli, M., and Guengerich, F. P. (2007) *Sulfolobus solfataricus* DNA polymerase Dpo4 is partially inhibited by "wobble" pairing between *O⁶*-methylguanine and cytosine, but accurate bypass is preferred. *J. Biol. Chem.* **282,** 1456–1467

39. Yuan, B., and Wang, Y. (2008) Mutagenic and cytotoxic properties of 6-thioguanine, *S⁶*-methylthioguanine, and guanine-*S⁶*-sulfonic acid. *J. Biol. Chem.* **283,** 23665–23670

40. Zhao, L., Christov, P. P., Kozekov, I. D., Pence, M. G., Pallan, P. S., Rizzo, C. J., Egli, M., and Guengerich, F. P. (2012) Replication of *N²*,3-ethenoguanine by DNA polymerases. *Angew. Chem. Int. Ed. Engl.* **51,** 5466–5469

41. Chowdhury, G., and Guengerich, F. P. (2011) Liquid chromatography-mass spectrometry analysis of DNA polymerase reaction products. *Curr. Protoc. Nucleic Acid Chem.* Chapter 7, Unit 7.16.1–11

42. Wickramaratne, S., Boldry, E. J., Buehler, C., Wang, Y. C., Distefano, M. D., and Tretyakova, N. Y. (2015) Error-prone translesion synthesis past DNA-peptide cross-links conjugated to the major groove of DNA via C5 of thymidine. *J. Biol. Chem.* **290,** 775–787

43. Chowdhury, G., and Guengerich, F. P. (2016) *Mass Spectrometry of Nucleic Acids*, in *Encyclopedia of Analytical Chemistry* (Meyers, R. A., ed) Wiley Interscience, New York, in press

44. Spencer, R. D., Weber, G., Tolman, G. L., Barrio, J. R., and Leonard, N. J. (1974) Species responsible for the fluorescence of 1:*N⁶*-ethenoadenosine. *Eur. J. Biochem.* **45,** 425–429

45. Inoue, Y., and Kuramochi, T. (1979) Protonation and quaternization of 1,*N⁶*-ethenoadenosine: what are the species responsible for the fluorescence of 1,*N⁶*-ethenoadenosine? *Biopolymers* **18,** 2175–2194

46. Singer, B., Antoccia, A., Basu, A. K., Dosanjh, M. K., Fraenkel-Conrat, H., Gallagher, P. E., Kuśmierek, J. T., Qiu, Z. H., and Rydberg, B. (1992) Both purified human 1,*N⁶*-ethenoadenine-binding protein and purified human 3-methyladenine-DNA glycosylase act on 1,*N⁶*-ethenoadenine and 3-methyladenine. *Proc. Natl. Acad. Sci. U.S.A.* **89,** 9386–9390

47. Saparbaev, M., Kleibl, K., and Laval, J. (1995) *Escherichia coli, Saccharomyces cerevisiae*, rat and human 3-methyladenine DNA glycolases repair 1,*N⁶*-ethenoadenine when present in DNA. *Nucleic Acids Res.* **23,** 3750–3755

48. Patra, A., Zhang, Q., Lei, L., Su, Y., Egli, M., and Guengerich, F. P. (2015) Structural and kinetic analysis of nucleoside triphosphate incorporation opposite an abasic site by human translesion DNA polymerase η. *J. Biol. Chem.* **290,** 8028–8038

49. Nair, D. T., Johnson, R. E., Prakash, L., Prakash, S., and Aggarwal, A. K. (2006) Hoogsteen base pair formation promotes synthesis opposite the 1,*N⁶*-ethenodeoxyadenosine lesion by human DNA polymerase ι. *Nat. Struct. Mol. Biol.* **13,** 619–625

50. Biertümpfel, C., Zhao, Y., Kondo, Y., Ramón-Maiques, S., Gregory, M., Lee, J. Y., Masutani, C., Lehmann, A. R., Hanaoka, F., and Yang, W. (2010) Structure and mechanism of human DNA polymerase η. *Nature* **465,** 1044–1048

51. Otwinowski, Z., and Minor, W. (1997) Processing of X-ray diffraction data collected in oscillation mode. *Methods Enzymol.* **276,** 307–326

52. Vagin, A., and Teplyakov, A. (2010) Molecular replacement with MOLREP. *Acta Crystallogr. D Biol. Crystallogr.* **66,** 22–25

53. Collaborative Computational Project No. 4 (1994) The CCP4 suite: Programs for protein crystallography. *Acta Crystallogr. D Biol. Crystallogr.* **50,** 760–763

54. Adams, P. D., Afonine, P. V., Bunkóczi, G., Chen, V. B., Davis, I. W., Echols, N., Headd, J. J., Hung, L. W., Kapral, G. J., Grosse-Kunstleve, R. W., McCoy, A. J., Moriarty, N. W., Oeffner, R., Read, R. J., *et al.* (2010) PHENIX: A comprehensive Python-based system for macromolecular structure solution. *Acta Crystallogr. D Biol. Crystallogr.* **66,** 213–221

55. Emsley, P., and Cowtan, K. (2004) Coot: model-building tools for molecular graphics. *Acta Crystallogr. D Biol. Crystallogr.* **60,** 2126–2132

56. Pettersen, E. F., Goddard, T. D., Huang, C. C., Couch, G. S., Greenblatt, D. M., Meng, E. C., and Ferrin, T. E. (2004) UCSF Chimera—a visualization system for exploratory research and analysis. *J. Comput. Chem.* **25,** 1605–1612